IOPscience iopscience.iop.org

Home Search Collections Journals About Contact us My IOPscience

Quantum-classical crossover for the biaxial spin model with field applied along the hard axis

This article has been downloaded from IOPscience. Please scroll down to see the full text article.

2000 J. Phys.: Condens. Matter 12 4243

(http://iopscience.iop.org/0953-8984/12/18/309)

View the table of contents for this issue, or go to the journal homepage for more

Download details:
IP Address: 171.66.16.221
The article was downloaded on 16/05/2010 at 04:53

Please note that terms and conditions apply.

J. Phys.: Condens. Matter **12** (2000) 4243–4251. Printed in the UK PII: S0953-8984(00)10018-9

Quantum–classical crossover for the biaxial spin model with field applied along the hard axis

X Martínez-Hidalgo†‡ and E M Chudnovsky‡

† Departament de Física Fonamental, Universitat de Barcelona, Diagonal 647, 08028 Barcelona, Spain

‡ Department of Physics and Astronomy, City University of New York–Lehman College, Bedford Park Boulevard West, Bronx, NY 10468-1589, USA

Received 30 November 1999, in final form 2 March 2000

Abstract. The quantum–classical crossover of the escape rate Γ of the biaxial spin model $\mathcal{H} = -DS_x^2 + ES_z^2 - g\mu_B S_z H_z$ is investigated in the exponential approximation with the help of the instanton technique. We find a new phenomenon in the dependence of Γ on temperature, namely a double transition (from thermal activation to thermally activated quantum tunnelling and then to ground-state quantum tunnelling). A new kind of spin thermon is also introduced in the formalism. The predictions can be tested experimentally for Fe_8 molecular nanomagnets.

1. Introduction

The escape rate of a particle from a metastable well is governed by two processes: quantum tunnelling through the barrier and thermal activation over it. The former dominates the rate at low temperatures, while the latter does so at high temperatures. Thus, in general, there is a crossover from one regime to the other as we change temperature. Quite generally, this crossover can be sharp (the so-called first-order transition) or smooth (second-order transition) [1].

For common metastable or double-well potentials, such as cubic or quartic parabolas, the second-order crossover is realized. Examples of systems and processes showing first-order crossover include superconducting quantum interference devices with two Josephson junctions [2], false vacuum decay in field theories [3–6], depinning of a massive string from a linear defect [7], and depinning of flux lines from columnar defects [8]. In the last few years, another process has drawn much attention: quantum–classical crossover in the rate of escape of a spin system out of a metastable well [9–17]. The reason is that the type of the crossover for these systems can be changed with an applied field. Consequently, the predictions of the theory can be relatively easily tested in experiment [18].

The dynamics of the spin system studied here can be adequately described by the spin Hamiltonian

$$\mathcal{H} = -DS_x^2 + ES_z^2 - g\mu_B \boldsymbol{S} \cdot \boldsymbol{H}. \tag{1}$$

The uniaxial case $E = 0$ has been the object of intensive study. The general biaxial case is of much interest, due to its relevance in the description of single-domain particles and high-spin molecules, such as Fe_8. The crossover diagram for the field directed perpendicular to the hard-magnetization axis has been recently studied by Kim [19]. In this article we study the

0953-8984/00/184243+09$30.00 © 2000 IOP Publishing Ltd

crossover in the biaxial case with an external field applied along the hard axis. This case has a non-trivial topology resulting in peculiar quantum interference effects [20–22]. We show that this topology produces a rich crossover diagram. As temperature is lowered, the system, in a certain field range, undergoes a second-order crossover followed by the first-order crossover. This prediction applies, in particular, to Fe_8 nanomagnets.

We use the instanton technique to compute the escape rate with exponential accuracy. The effect of the prefactor is not computed explicitly, though it is expected to smooth the crossover (with the result that all derivatives of Γ at the crossover become continuous) and to modify slightly the transition temperature; see reference [11] for details. For a moderate spin of Fe-8, $S = 10$, the first- and second-order crossover refer to the difference in temperature dependence of the magnetic quantum number, m, that dominates the rate of the magnetic relaxation [9,18]. We will restrict our considerations to the moderate-damping regime, where the rate is damping independent.

The structure of the main part of this article is the following. In section 2 the fundamentals concerning the instanton approach and the derivation of the effective potential are reviewed. In section 3 the escape rate is studied in the exponential approximation and the crossover diagram is worked out for the general biaxial Hamiltonian. In section 4 the results of section 3 are applied to the octanuclear iron cluster Fe_8 and experiments are suggested for the observation of the different types of crossover. The main results obtained in this work are discussed in section 5.

2. Effective potential and escape rate

The starting point for the instanton approach (for a review of the method, see for instance reference [23] and references cited therein) is the formula for the escape rate [24]

$$\Gamma = \frac{2T}{\hbar}\frac{\mathrm{Im}(Z)}{\mathrm{Re}(Z)} \tag{2}$$

where the partition function Z can be evaluated as the functional integral

$$\oint \mathcal{D}[\cos\theta(\tau)]\,\mathcal{D}[\phi(\tau)]\,\exp\left(-\frac{1}{\hbar}\int \mathrm{d}\tau\ \mathcal{L}_E[\theta(\tau),\phi(\tau)]\right) \tag{3}$$

over all trajectories $x(\tau)$ that are periodic in imaginary time with the period $\tau_p = \hbar/T$. Here $\mathcal{L}_E = -\mathcal{L}(t \to -\mathrm{i}\tau)$ is the Euclidean Lagrangian that has the form

$$\mathcal{L}_E = \mathrm{i}\hbar S(\cos(\theta) - 1)\dot{\phi}_\tau + \mathcal{H}(\theta,\phi) \tag{4}$$

where $\mathcal{H}$ is the classical energy of the system corresponding to the quantum Hamiltonian (1). In this model it is given by

$$\mathcal{H}(\theta,\phi) = KS^2[\cos^2(\theta) + \lambda\sin^2(\theta)\sin^2(\phi) - 2h\cos(\theta) + h^2] \tag{5}$$

where $K = D + E$, $\lambda = D/(D+E)$, $h = H/H_c$ and $H_c = 2S(D+E)/(g\mu_B)$ is the critical field in the Z-direction. For $h < 1$ the energy $\mathcal{H}(\theta,\phi)$ has two equivalent minima at $\phi = 0, \pi$ with $\cos(\theta) = h$. A constant has been added to make the energy of these minima zero.

After Gaussian integration over $\cos(\theta)$ in equation (3), one can express the partition function as

$$\oint \mathcal{D}[\phi(\tau)]\,\exp\left(-\frac{1}{\hbar}S_E[\phi(\tau)]\right) \tag{6}$$

where the Euclidean action S_E is given by

$$S_E[\phi(\tau)] = \mathrm{i}\hbar\int \mathrm{d}\phi\ [A(\phi) - S] + \int \mathrm{d}\tau\ \left[\frac{1}{2}M(\phi)\dot{\phi}_\tau^2 + V(\phi)\right] \tag{7}$$

and the effective 'vector' potential $A(\phi)$, mass $M(\phi)$ and potential $V(\phi)$ are

$$A(\phi) = \frac{hS}{1 - \lambda \sin^2(\phi)} \tag{8}$$

$$M(\phi) = \frac{1}{2K[(1 - \lambda \sin^2(\phi)]} \tag{9}$$

and

$$V(\phi) = KS^2\lambda \sin^2(\phi)\left[1 - \frac{h^2}{1 - \lambda \sin^2(\phi)}\right]. \tag{10}$$

The first term in equation (7) is the topological Wess–Zumino–Berry phase which contributes solely to the imaginary part of S_E [20, 25, 26]. This is responsible for interference effects at zero temperature. As the tunnelling variable is mesoscopic ($S = 10$), the real part of the imaginary-time action is likely to be large compared to $\hbar$. Thus the path integral can be evaluated using a saddle-point approximation to obtain the semiclassical result. The escape rate has then the general form $\Gamma(T) = A(T)\exp[-B(T)]$, where $B(T)$ is given by

$$B(T) = \mathrm{Re}\left(\frac{1}{\hbar}S_E[\phi(\tau)]\right) = \mathrm{Re}\int \mathrm{d}\tau \ \left[\frac{1}{2}M(\phi)\dot{\phi}_\tau^2 + V(\phi)\right] = J(E) + E/T \tag{11}$$

$$J(E) = \mathrm{Re}\oint p \, \mathrm{d}\phi = \int \mathrm{d}\phi \ \{2M(\phi)[V(\phi) - E]\}^{1/2}. \tag{12}$$

Here the integral is to be evaluated along the trajectory $\phi(\tau)$ which minimizes the action S_E. We can identify two contributions: the term $\exp[-J(E)]$, which is the transparency of the barrier for the thermon trajectory, and the term $\exp(-E/T)$, which is the Boltzmann factor giving the thermal population for the level that dominates the escape rate.

The shapes of the potential $V(\phi)$ for three different ranges of the field are shown in figure 1. For $h < h_1 = 1 - \lambda$, the potential looks like a normal barrier between $\phi = 0$ and $\phi = \pi$, with a maximum at $\phi = \pi/2$. For $h_1 < h < h_2 = (1 - \lambda)^{1/2}$, the maximum at $\phi = \pi/2$ becomes a local minimum, though still higher than the global minima at $\phi = 0, \pi$. For $h_2 < h < 1$, the minimum at $\phi = \pi/2$ becomes the global minimum. The barrier height is

$$\Delta V \equiv V_{\max} - V(0) = \begin{cases} KS^2\lambda\left[1 - h^2/(1 - \lambda)\right] & \text{if } 0 < h < h_1 \\ KS^2(1 - h)^2 & \text{if } h_1 < h < 1. \end{cases} \tag{13}$$

For $h_1 < h < 1$ the non-standard shape of the potential might give rise to some ambiguity in the definition of the thermon. We shall discuss one concrete example. Let us consider the case $h_2 < h < 1$ and a trajectory with energy E such that $0 < E < V_{\max}$. Such a trajectory is shown in figure 1. The trajectory that we should consider for the computation of B is the one joining ϕ_1 and $\pi - \phi_1$, which consists of three parts:

(i) motion in imaginary time from ϕ_1 to ϕ_2,
(ii) motion in real time from ϕ_2 to $\pi - \phi_2$,
(iii) motion in imaginary time from $\pi - \phi_2$ to $\pi - \phi_1$.

The real-time part of the trajectory gives a purely imaginary contribution to the Euclidean action and is responsible for the destruction of interference at zero temperature (unfreezing of tunnelling) [21]. The other two parts of the trajectory contribute exactly the same amount to the real part of the action. This 'mixed-time' thermon is consistent with the usual picture in which the particle must tunnel from one side to the other of the barrier. It also agrees with the instanton introduced in reference [21] in the limit $T \to 0$.

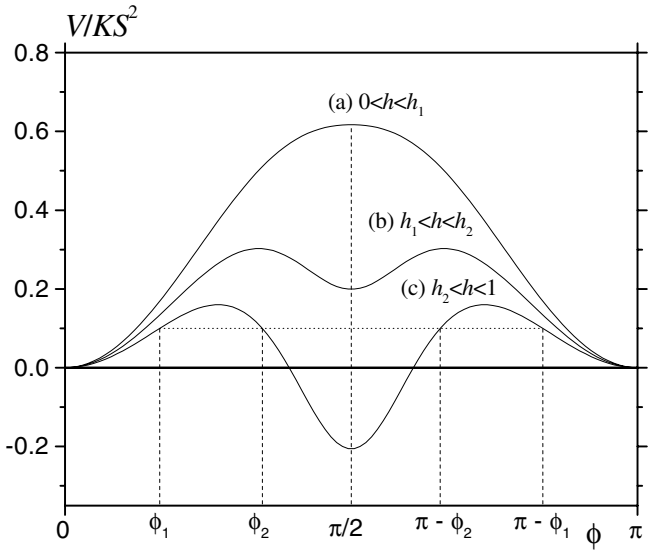

Figure 1. The potential $V(\phi)$ at $\lambda = 0.72$ ($h_1 = 0.28$ and $h_2 \approx 0.529$) for three different ranges of the field. The chosen fields are: (a) $h = 0.2$, (b) $h = 0.45$ and (c) $h = 0.6$. The dotted line corresponds to the thermon trajectory discussed in the text.

3. Quantum–classical transition in the exponential approximation

In the exponential approximation we neglect the prefactor in the expression for the escape rate Γ, so

$$\Gamma \sim \exp[-B(T)].$$

To determine $B(T)$ one must find the periodic trajectory $\phi(\tau)$ which is the solution of the equation of motion in the inverted potential and has an energy E which minimizes the effective 'free energy'

$$F(T, E) = T\,B(E) = E + T\,J(E). \tag{14}$$

A necessary condition is that E is an extremum of F, or equivalently

$$\frac{\partial F(T, E)}{\partial E} = 0 \Rightarrow \tau(E) = \frac{1}{T}$$

where $\tau(E) = -\mathrm{d}J(E)/\mathrm{d}E$ is the period of oscillations in the inverted potential $-V(x)$. In the case where $\tau(E)$ is a non-monotonic function of E, this equation might have several solutions. To this, one must also add the solution $E = V_{\max}$, which gives $F(E) = \Delta V$, corresponding to the overbarrier transition by thermal activation. When there are several solutions, one must choose the one corresponding to the global minimum of $F(E)$. Consequently, to compute $B(T)$ we need to compute $J(E)$ and its derivative, which can be done using expression (12) (the integral can be evaluated numerically).

3.1. Crossover diagram. Types of crossover

After analysing $B(T)$ for different values of h and λ we find different types of quantum–classical crossover in different regions of the crossover diagram (see figures 2 and 3). Physically, the different types of crossover arise from the interplay between two competing

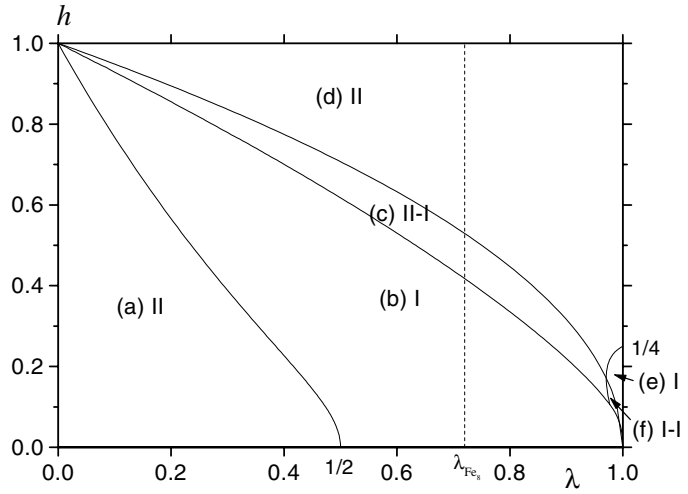

Figure 2. A crossover diagram showing the different types of crossover as functions of h and λ. The dashed line shows the relevant section for Fe_8.

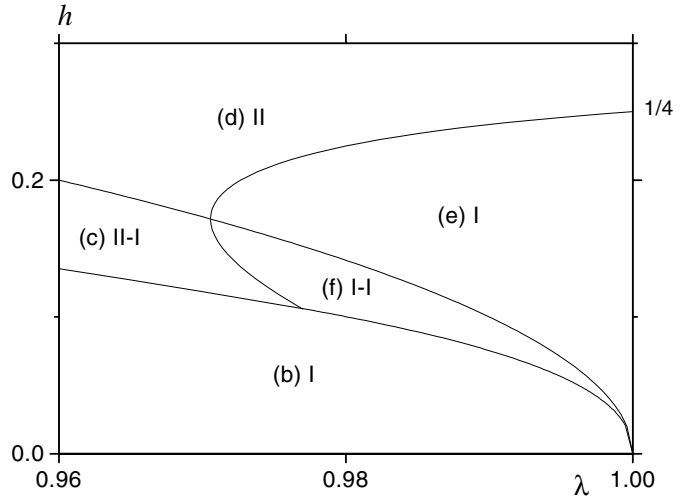

Figure 3. Details of the crossover diagram in the high-field region.

effects, namely the change in thermal population and the change of the transparency of the barrier as we consider different tunnelling levels. Whereas the former decrease exponentially according to the Boltzmann factor as we consider more energetic levels, the latter behaves in the opposite way. As the barrier has a non-trivial shape (due to the low symmetry of the spin Hamiltonian), we can observe several behaviours of the quantum rate near the crossover. We now proceed to discuss the different types of crossover obtained in this system.

3.1.1. Second-order crossover (II). In regions (a) and (d), we have a second-order crossover from thermal activation (TA) to thermally assisted quantum tunnelling (TAQT) near the top of the barrier. This can be deduced from the fact that the period τ increases monotonically with decreasing energy E. In this case, the energy E of the level which dominates the escape rate

or, equivalently, the value of the order parameter P defined by

$$P \equiv \frac{V_{\max} - E}{\Delta V}$$

changes continuously when we go from one regime (TA, $P = 0$) to the other (TAQT, $P > 0$). The crossover temperature can be computed exactly, giving

$$T_0^{(2)} = \frac{\tilde{\omega}_0}{2\pi} = \begin{cases} \dfrac{KS}{\pi}\sqrt{\dfrac{\lambda[(1-\lambda)^2 - h^2]}{1-\lambda}} & \text{if } 0 < h < h_1 \\ \dfrac{KS}{\pi}\sqrt{(1-h)[h-(1-\lambda)]} & \text{if } h_1 < h < 1 \end{cases} \tag{15}$$

where $\tilde{\omega}_0$ is the frequency of small oscillations around the top of the barrier in the inverted potential. In the second case ($h_1 < h < 1$), a factor of $1/2$ has been added to take into account that there is a double barrier.

3.1.2. First-order crossover (I). In regions (b) and (e), we have a first-order crossover from thermal activation (TA) to thermally assisted quantum tunnelling near the ground state (QT). Here the period τ does not depend monotonically on the energy and we find that the crossover takes place at $T_0 > T_0^{(2)}$. In this case, P changes discontinuously when we go from one regime (TA) to the other (QT). The two trajectories that compete in the determination of the escape rate are the one at the top of the barrier, with $B(T) = \Delta U/T$, and the one near $E = 0$, with $B \approx J(0)$. Thus we can estimate the crossover temperature using the expression

$$T_0^{(1)} = \frac{\Delta U}{J(0)} = \begin{cases} KS\lambda\left\{4\tilde{a}^2\left[\sinh^{-1}\left(\dfrac{\tilde{a}}{b}\right) - \left(1 - \dfrac{1}{\tilde{a}^2}\right)^{1/2}\coth^{-1}\left(\dfrac{\tilde{a}^2 + b^2}{\tilde{a}^2 - 1}\right)^{1/2}\right]\right\}^{-1} \\ \qquad \text{if } 0 < h < h_1 \\ KS(1-h)^2\left\{4\left[\cosh^{-1}\left(\dfrac{a}{b}\right) - \left(1 + \dfrac{1}{a^2}\right)^{1/2}\tanh^{-1}\left(\dfrac{a^2 - b^2}{a^2 + 1}\right)^{1/2}\right]\right\}^{-1} \\ \qquad \text{if } h_1 < h < 1 \end{cases} \tag{16}$$

where

$$a^2 = -\tilde{a}^2 = \frac{1-\lambda}{h^2 - (1-\lambda)} \qquad b^2 = \frac{1-\lambda}{\lambda} = \frac{E}{D}. \tag{17}$$

3.1.3. Second-order crossover followed by first-order crossover (II–I). The two previous types of crossover can also be found in the uniaxial spin case. However, in the biaxial case we find a new type of crossover. In region (c), the system suffers a second-order crossover from thermal activation (TA) to thermally assisted quantum tunnelling near the top of the barrier (TAQT) at $T_0^{(2)}$ and then, at a lower temperature $T_0^{(1)}$, it undergoes a first-order crossover from TAQT to thermally assisted quantum tunnelling near the ground state (QT). The period τ has a complicated dependence on E (it is not monotonic). In this case, P changes continuously at $T_0^{(2)}$ when we go from TA to QT and discontinuously at T_0 when we go from TAQT to QT. The temperature for the second-order crossover is given exactly by equation (15). The temperature for the first-order crossover $T_0^{(1)} < T_0^{(2)}$, though, cannot be estimated with the expression (16), because here the ground-state tunnelling does not compete directly with thermal activation; instead it competes with thermally activated tunnelling at some energy above $V(\pi/2)$.

3.1.4. First-order crossover followed by first-order crossover (I–I). There is another type of crossover which occurs in the biaxial model but not in the simpler uniaxial one: in region (f), the system suffers a first-order crossover from thermal activation (TA) to thermally assisted quantum tunnelling at some energy $E > V(\pi/2)$ (TAQT) at $T_0^{(1a)}$ and then, at a lower temperature $T_0^{(1b)}$, it undergoes a first-order crossover from TAQT to thermally assisted quantum tunnelling near the ground state (QT). The period τ is again not monotonic on E. Now P changes discontinuously both at $T_0^{(1a)}$ when we go from TA to QT and at $T_0^{(1b)}$ when we go from TAQT to QT. As in the previous case, expression (16) does not give us a good estimate of any of the crossover temperatures for similar reasons.

3.2. Crossover boundaries

Some of the boundaries between the different regions in the crossover diagram of figure 2 can be computed analytically. The boundary between regions (a) and (b) is given by the condition

$$\left.\frac{\mathrm{d}\tau(P)}{\mathrm{d}P}\right|_{P=0^+} = 0. \tag{18}$$

This condition gives

$$h(\lambda) = (1-\lambda)\sqrt{\frac{1-2\lambda}{1+\lambda}}. \tag{19}$$

In the case of zero field $h = 0$, one gets $\lambda = 1/2$, which agrees with previous results.

The boundary between region (b) and (c) can be determined numerically from the condition

$$F(T_0^{(2)}, E_0) = F(T_0^{(2)}, V_{\max}) \tag{20}$$

where E_0 is the energy of the trajectory near the ground state that minimizes F at $T_0^{(2)}$. The boundary between region (b) and (f) can be calculated in a similar way using the condition

$$F(T_0^{(1a)}, E_a) = F(T_0^{(1a)}, E_b) \tag{21}$$

where E_a and E_b are the energies of the trajectories above and below $V(\pi/2)$, respectively, that minimize F at $T_0^{(1a)}$.

The line that separates region (c) from (d) and region (e) from (f) is given by $h(\lambda) = h_2 = (1-\lambda)^{1/2}$. Finally, one can also compute the equation of the boundary between regions (d) and (e) and between (c) and (f). It is also given by condition (18), which gives in this case

$$h(\lambda) = \frac{16 + \lambda^2 - \lambda\left(16 \pm \sqrt{-32 + 32\lambda + \lambda^2}\right)}{8(2-\lambda)}. \tag{22}$$

Note that in the uniaxial case $\lambda = 1$, one recovers the known result $h = 1/4$ separating the first-order crossover from the second-order crossover.

4. Special case: Fe_8

One of the systems where this theory could be tested is the molecular magnet Fe_8. In this section we apply the results of the previous section to this system. For Fe_8, $S = 10$, $K \approx 0.34$ K and $\lambda \approx 0.72$. The critical field in the Z-direction is $H_c \approx 5.1$ T. The dashed line in figure 2 shows the regions of the crossover diagram relevant to this system. We can observe that for Fe_8 there is no field range in which the crossover of the type (I–I) occurs. The other types of crossover do occur at different regions of field. The crossover temperature as a function of field for this system has been computed exactly in the exponential approximation and is shown in figure 4. The field H_3, separating the crossover type (I) from the crossover type (II–I) can be computed numerically, and is $H_3 \approx 2.1$ T. We also have $H_2 = h_2 H_c \approx 2.7$ T. Note that for Fe_8 the escape rate in the region (II–I) should be in the GHz range.

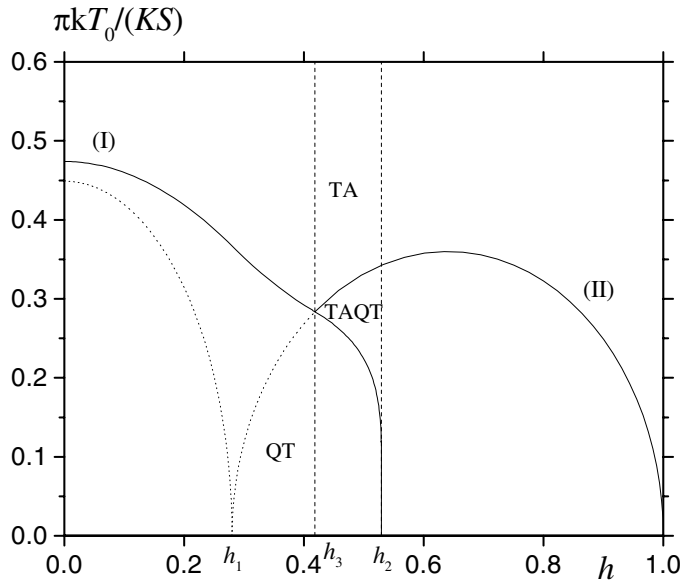

Figure 4. Crossover temperature as a function of reduced field h for $\lambda = 0.72$ (the relevant value for Fe_8). The highlighted fields $h_2 = (1-\lambda)^{1/2}$ and $h_3 \approx 0.42$ are the boundaries between the (I)-, (II–I)- and (I)-type crossover. The field $h_1 = 1 - \lambda$ is the point where the top of the barrier splits in two.

5. Discussion

We have presented a study of the quantum–classical crossover of the escape rate of a biaxial spin model with the field applied along the hard axis. We have considered the exponential approximation and restricted our considerations to the moderate-damping regime. The method employed is the instanton technique. A new kind of spin thermon has been introduced in the formalism to allow the analysis of the crossover in this model. The resulting crossover diagram shows that the variety of different types of crossover in the biaxial model is much richer than in the uniaxial case. Besides the known first-order and second-order types of crossover, we have found two more types of crossover: (II–I) and (I–I). The crossover temperature has been computed for the different types of quantum–classical transition.

These results have been applied to the high-spin molecule Fe_8. The results are also relevant to the study of small particles. In that case, though, a longitudinal field must also be applied to lower the barrier, so a generalization of the present work to the arbitrarily directed field would be of interest. (The case with a longitudinal field only has been recently studied using a perturbative approach [27].)

Acknowledgments

The work of EMC was supported by the US National Science Foundation under the Grant No DMR-9978882. XMH acknowledges support from the Comissionat per a Universitats i Recerca of the Generalitat de Catalunya.

References

[1] Chudnovsky E M and Tejada J 1998 *Macroscopic Quantum Tunnelling of the Magnetic Moment* (Cambridge: Cambridge University Press)
[2] Morais-Smith C, Ivlev B and Blatter G 1994 *Phys. Rev.* B **49** 4033
[3] Garriga J 1994 *Phys. Rev.* D **49** 5497
[4] Ferrera A 1995 *Phys. Rev.* D **52** 6717
[5] Habib S, Mottola E and Tinyakov P 1996 *Phys. Rev.* D **54** 7774
[6] Zimmerschied F, Tchrakian D H and Müller-Kirsten H J W 1998 *Fortschr. Phys.* **46** 147
[7] Skvortsov M A 1997 *Phys. Rev.* B **55** 515
[8] Gorokhov D A and Blatter G 1997 *Phys. Rev.* B **56** 3130
Gorokhov D A and Blatter G 1997 *Phys. Rev.* B **57** 3577
Gorokhov D A and Blatter G 1998 *Phys. Rev.* B **57** 3586
Gorokhov D A and Blatter G 1998 *Phys. Rev.* B **58** 5486
[9] Garanin D A and Chudnovsky E M 1997 *Phys. Rev.* B **56** 11 102
[10] Chudnovsky E M and Garanin D A 1997 *Phys. Rev. Lett.* **79** 4469
[11] Garanin D A, Martínez-Hidalgo X and Chudnovsky E M 1998 *Phys. Rev.* B **57** 13 639
[12] Liang J-Q, Müller-Kirsten H J W, Park D K and Zimmerschied F 1998 *Phys. Rev. Lett.* **81** 216
[13] Lee S-Y, Müller-Kirsten H J W, Park D K and Zimmerschied F 1998 *Phys. Rev.* B **58** 5554
[14] Choi T and Kim G-H 2000 *J. Phys.: Condens. Matter* submitted
[15] Kim G-H 2000 *J. Appl. Phys.* **86** 1062
[16] Kou S P, Liang J-Q, Zhang Y B, Wang X B and Pu F C 1999 *Phys. Rev.* B **59** 6309
[17] Zhang Y B, Liang J-Q, Müller-Kirsten H J W, Kou S P, Wang X B and Pu F C 2000 *Phys. Rev.* B **60** 12 886
[18] Kent A D, Zhong Y, Bokacheva L, Ruiz D, Hendrickson D N and Sarachik M P 2000 *Europhys. Lett.* **49** 521
[19] Kim G-H 1999 *Phys. Rev.* B **59** 11 847
[20] Garg A 1993 *Europhys. Lett.* **22** 205
[21] Chudnovsky E M and Martínez-Hidalgo X 2000 *Europhys. Lett.* at press
[22] Wernsdorfer W and Sessoli R 1999 *Science* **284** 133
[23] Gunther L and Barbara B (ed) 1994 *QTM'94: Quantum Tunneling of Magnetization* (Dordrecht: Kluwer–Academic)
[24] Langer J S 1967 *Ann. Phys., NY* **41** 108
[25] von Delft J and Henley C L 1992 *Phys. Rev. Lett.* **69** 3236
[26] Loss D, DiVincenzo D P and Grinstein G 1992 *Phys. Rev. Lett.* **69** 3232
[27] Garanin D A and Chudnovsky E M 1999 *Phys. Rev.* B **59** 3671